MNRAS 000, 1–5 (2022) Preprint 29 November 2024 Compiled using MNRAS LATEX style file v3.0

The effects of feedback on baryonic halo mass relations in CAMELS

Noam J. Scully[1]★
[1]Department of Astronomy, Yale University, 52 Hillhouse Avenue, New Haven 06520, USA

29 November 2024

ABSTRACT

The stellar-halo mass relation (SHMR) relates a halo's mass to its stellar fraction, and has an important application in baryon pasting, a technique for fast, accurate simulations. However, we hypothesize that the SHMR changes with feedback strength; and that in applications like baryon pasting, the equational form of the SHMR should change to reflect this. We test this in the CAMELS set of simulations, comparing the SHMR in boxes with extremely high or low feedback levels, and find that increased supernova feedback reduces stellar fractions. We repeat this analysis on other halo mass relations—replacing the stellar fraction with gas or total baryonic fraction—and find a nonmonotonic relationship between supernova feedback and the gas fraction, suggesting nonlinear mechanisms involved in feedback. Finally, we discuss our effort to quantify the SHMR's dependence on feedback.

Key words: software: simulations

1 INTRODUCTION

Simulations play a central role in modern astrophysics and cosmology research, helping put observations in context, connect them to the physical models they might indicate, and probe physics that we cannot observe directly. However, the two commonly used types of simulations each have drawbacks. *N-body simulations* only implement gravitational forces between mass particles. As a result, they run quickly, but sacrifice accuracy, with too much matter falling to the core of simulated halos. Meanwhile, *hydrodynamic simulations* include electromagnetic effects like feedback in addition to gravity. This takes considerably more computing resources but results in simulations that better reflect our universe.

A current frontier of the field is to achieve the speed and flexibility of an N-body simulation and the accuracy of a hydrodynamic simulation. One promising candidate is *baryon pasting*, which involves starting with an N-body simulation, and then layering baryons on top according to a set of equations that describe how they evolve and distribute themselves at large scales. This saves significant time by doing away with granular calculations of interacting baryons seen in hydrodynamic simulations.

Our long-term goal is to implement baryon pasting to mimic the Cosmology and Astrophysics with MachinE Learning Simulations (CAMELS). CAMELS is a set of simulations designed to explore universes with a wide variety of cosmological and astrophysical properties. In lieu of simulating especially large regions of space, CAMELS favors simulating a higher number of relatively smaller volumes; that makes it well-suited to finding patterns across boxes, which are the types of relationships used in baryon pasting.

In this report, we focus on one such relationship, the *stellar-halo mass relation* (SHMR). The SHMR captures how the size of a halo relates to the fraction of its mass composed of stars. Written as an equation, the SHMR is of the form $M_*/M_h = f(M_h)$, where M_h is halo mass, M_* is stellar mass, and f is some function. However, we hypothesize that in CAMELS simulations with different physics—specifically, differing levels of feedback—the SHMR changes substantially enough that a single equation cannot adequately model it for every simulation at once. Instead of only relating stellar mass to halo mass, we seek a functional form that also depends on the parameters that control CAMELS's feedback (see Table 1 for details about the parameters):

$$\frac{M_*}{M_h} = f(M_h, A_{SN1}, A_{SN2}, A_{AGN1}, A_{AGN2}). \quad (1)$$

In this report, we paint a qualitative picture of how stellar mass changes with feedback strength. Alongside the SHMR, we look at how other, less-studied halo mass relations respond to feedback. Comparing the fraction of gas mass to a halo's total mass gives what we dub the *gas-halo mass relation* (GHMR). Comparing the total baryonic fraction—the sum of stellar and gas mass—to the halo's total mass gives the *baryonic-halo mass relation* (BHMR). In addition to being informative about a wider scope of matter in their own right, analyzing the GHMR and BHMR will give insight into the feedback physics driving changes in the SHMR.

2 METHODS

2.1 CAMELS

CAMELS contains 4233 simulations, or *boxes*. Each box follows a cubic region of space with side length 25 Mpc h^{-1}—large enough to contain halos of up to ~$10^{14} M_\odot$—from $z = 6$ to $z = 0$. These boxes come in two types: N-body simulations, which only implement gravitational forces between mass particles; and hydrodynamic

★ E-mail: noam.scully@yale.edu

Table 1. The four CAMELS feedback parameters.

Parameter	*Range*	*Value it scales*
A_{SN1}	[0.25,4]	In IllustrisTNG, energy output per unit star formation; in SIMBA, mass outflow rate per unit star formation.
A_{AGN1}	[0.25,4]	In IllustrisTNG, power output of AGN feedback in 'kinetic' mode; in SIMBA, momentum flux of mass outflows.
A_{SN2}	[0.5,2]	Galactic wind speed in IllustrisTNG and SIMBA.
A_{AGN2}	[0.5,2]	In IllustrisTNG, temperature of feedback bursts; in SIMBA, speed of continuous feedback jets.

simulations, which include electromagnetic effects like cooling, star-formation, and feedback in addition to gravity. Boxes also fall into two categories based on the type of code they run on: CAMELS uses frameworks from two recent sets of simulations, IllustrisTNG and SIMBA, in different boxes. The final variations in boxes are due to their individual setups. This includes their starting distribution of matter as well as the values of six parameters that alter the physics of each box.

We analyze a subset of 61 hydrodynamic boxes called 1P, which stands for "1 parameter at a time". 1P contains a *fiducial* box, in which all six parameters are set to baseline values. The remaining 60 boxes share initial conditions and 5 out of 6 parameter values with the fiducial box, but the value of the final parameter varies, incremented upwards in five boxes and downwards in five boxes. This gives a spread of eleven boxes for each parameter, and any variation across the spread must result from that parameter's changing value.

Of the six parameters varied in CAMELS, we focus on the four shown in Table 1, which control aspects of supernova (SN) feedback or active galactic nuclei (AGN) feedback. Note that the physical meanings differ for boxes based on IllustrisTNG versus on SIMBA.

2.2 Calculating Halo Mass Relations

To find the halo mass relation for a given quantity q (stellar mass, gas mass, or total baryonic mass) in a given box, we first calculate the mass of q in each of the box's halos. For each halo, we find the quantity's density δ_q out to 25 logarithmically spaced radii, denoted r_n. We approximate the cumulative mass of q out to r_n by summing the mass of q in successive spheres out to r_n,

$$M_q(r_n) = \frac{4\pi}{3} \sum_{i=1}^{n} \delta_q(r_i) r_i^3 . \quad (2)$$

Note that the spheres are concentric, so lower-radius spheres contribute their volume multiple times; however, the exponential growth of r_n renders those extra contributions negligible. Let r_h be the closest r_n to a given halo's r_{200c}. We define the total mass of q in that halo as $M_q = M_q(r_h)$.

Next, we sort the box's halos into 10 logarithmically spaced bins based on their total mass $M_h = M_{200c}$. Call the medians of M_h and M_q in the kth mass bin M_{h_k} and M_{q_k}. The 10 median data points of the form $(M_{h_k}, M_{q_k}/M_{h_k})$ then give q's halo mass relation. In our halo mass relation figures (Figs. 1, 2, 3, and 4) the trendlines show these median points, and the shaded scatters show one standard deviation away from the median (the 16th and 84th percentile values of M_{q_k}/M_{h_k} within each mass bin).

2.3 Fitting the SHMR

We find lines of best fit for the SHMR in 1P boxes that vary A_{SN1} or A_{SN2} at several different redshifts. Each fit follows a double power law form based on those in Moster et al. 2010 and Girelli et al. 2020:

$$\frac{M_\odot}{M_h} = 2A \cdot \left(\left(\frac{M_h}{M_A} \right)^{-\beta} + \left(\frac{M_h}{M_A} \right)^{\gamma} \right) . \quad (3)$$

The four parameters β, γ, M_A, and A control the shape of the curve: when $M_h < M_A$, the slope is mostly determined by β; when $M_h > M_A$, the slope is mostly determined by γ; and when $M_h \approx M_A$, the stellar fraction is approximately A. We generate the best-fit parameters in each box using `scipy.optimize.curve_fit` with an initial guess of `(1, 1, 1, 1e11)` for (A, β, γ, M_A).

3 CONCLUSIONS

3.1 Halo Mass Relations

3.1.1 Stellar-Halo Mass Relation

Figure 1 shows the SHMR for several 1P boxes. The fiducial box is shown in black, and each different color shows the boxes with the extreme high value or extreme low value of each parameter. The two plots show boxes run on IllustrisTNG and those run on SIMBA. In IllustrisTNG and SIMBA, the trendlines for A_{SN1} and A_{SN2} deviate from the fiducial trendline. This is likely because when either of those parameters is high, feedback introduces more thermal energy to the halos' gas, preventing cooling and star formation. On the other hand, lowering parameter values has the opposite effect, allowing for more cooling and higher stellar fractions. Both these effects are less pronounced in SIMBA than in IllustrisTNG.

In contrast, the two AGN feedback parameters hardly deviate from the fiducial simulation in both SIMBA and IllustrisTNG. Further exploration is needed to understand why AGN parameters do not impact the SHMR in this case.

3.1.2 Gas-Halo Mass Relation

The GHMR in CAMELS has less clear dependence on all four feedback parameters than the SHMR. First, increasing A_{SN1} causes a higher gas fraction, especially in high mass halos in case of IllustrisTNG. This is likely due to gaseous mass cooling into stellar mass when it receives less energy from feedback. Conversely, A_{AGN2} only has a pronounced effect in SIMBA; increasing its value decreases the gas fraction in high-mass halos. Since A_{AGN2} controls jet speed in SIMBA, this may reflect gas exceeding the escape velocity of its halo—but we would expect to see this occur more in small halos, not large ones. In both types of simulations, A_{AGN1} does little to alter the gas fraction. However, the differences between IllustrisTNG and SIMBA, as well as the large overlaps in scatters, mean that all these results merit more investigation to confirm or disprove—for example, by extending the analysis to CAMLES boxes outside of 1P.

Lastly, Figure 3 shows A_{SN2}'s effect on the GHMR. Surprisingly, the low and high value trendlines intersect around $10^{12.2} M_\odot$; in other words, setting this parameter to its extreme high or extreme low values has the same effect, but at different mass ranges. We theorize that this non-monotonicity comes from feedback loops that dictate the amount of stellar feedback in a halo. Specifically, at low halo mass, a high value of A_{SN2} accelerates gas to above escape velocity, while at high halo mass, increased star formation from low

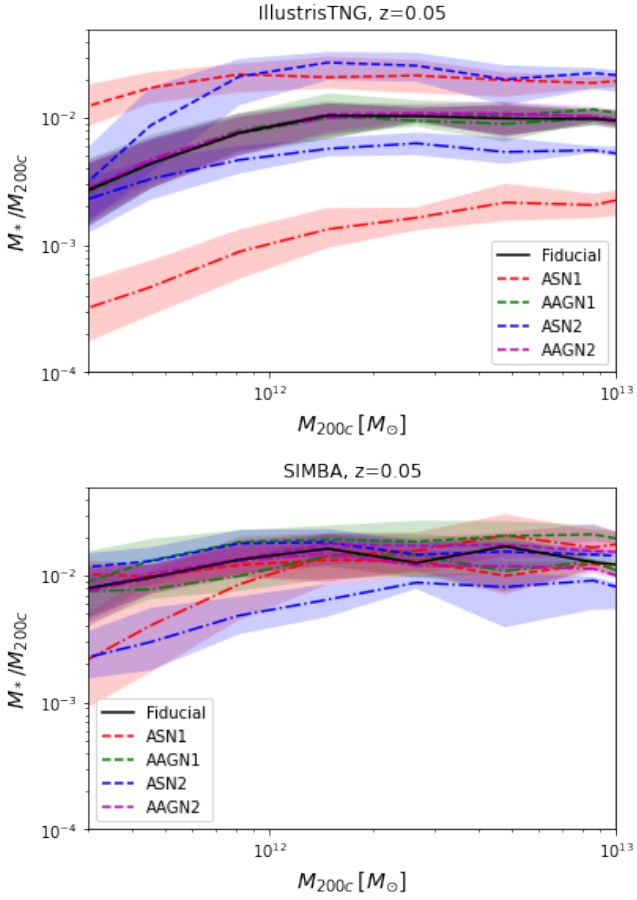

Figure 1. Each trendline shows the median SHMR in a 1P box, with halo mass on the x-axis and stellar fraction on the y-axis. The scatter shows one standard deviation. The black line is the fiducial simulation; dashed lines show boxes with the lowest values of each parameter; dot-dash lines show boxes with the highest values. The two plots show IllustrisTNG boxes and SIMBA boxes separately.

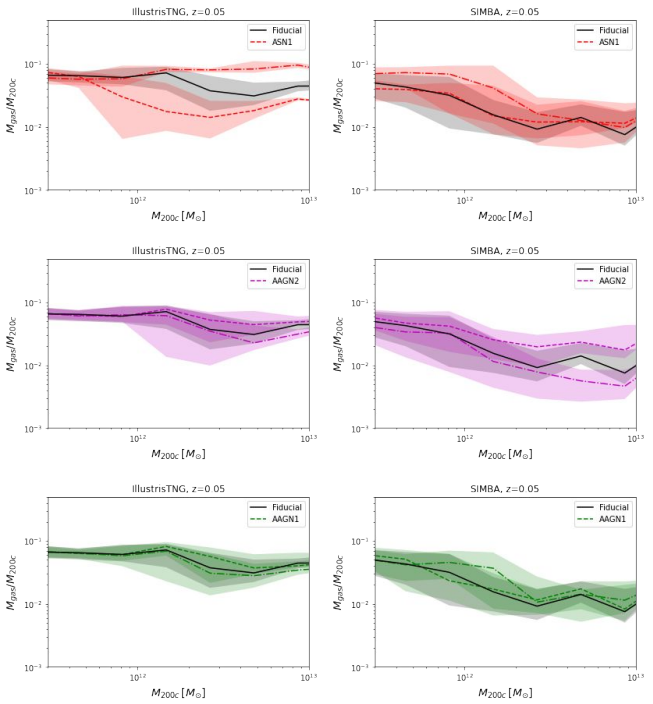

Figure 2. Each trendline shows the median GHMR in the fiducial 1P box and in the 1P boxes with lowest (dashed) and highest (dot-dashed) values of A_{AGN1}, A_{AGN2}, or A_{SN1}. The scatter shows one standard deviation. Unlike the SHMR, the GHMR is sensitive to A_{AGN2}.

A_{SN2} leads to more supernova events that expel gas. As a future step, we plan to test this hypothesis by looking at amounts of gas lying beyond halos' virial radius.

3.1.3 Baryonic-Halo Mass Relation

In a typical 1P box, the median halo's gas fraction is about one order of magnitude higher than its stellar fraction. Because of this, the BHMR, which is the sum of the SHMR and GHMR, closely resembles the GHMR alone. For example, Fig. 4 and Fig. 3 share most of their features; notably, both have an intersection between high and low A_{SN2} values in IllustrisTNG.

However, greater overlap between scatters makes the intersection less significant in the BHMR than the GHMR. Likewise, SIMBA's BHMR trendlines stay closer to the fiducial line than in the GHMR SIMBA figures. This convergence towards the fiducial line occurs because at most halo masses, A_{SN2}'s value has opposite effects on the stellar and gas fractions: low A_{SN2} produces higher stellar mass and lower gas mass; high A_{SN2} produces lower stellar mass and higher gas mass. When summed, these opposing effects cancel, bringing the total baryonic fraction closer to fiducial amounts. This indicates that looking at the baryonic fraction alone would mask the true extent of variation that A_{SN2} causes—some amount of baryons remain within the halo as A_{SN2} changes, but transfer from being gaseous to being stellar (or vice versa). A_{SN1} similarly produces cancellation between stellar and gas fractions, so the same caveat applies.

3.2 SHMR Best Fits with z Dependence

We quantified the dependence of stellar mass on feedback by fitting the SHMR to a double power law, which is the standard SHMR fit in prior work (e.g. Girelli et al. 2020, Moster et al. 2010). For the eleven boxes that varied A_{SN1} and A_{SN2}, we plot the best-fit values and standard deviations of β, γ, M_A, and A at five redshifts from $z = 0$ to $z = 2$. Figure 5 shows these plots for the normalization factor A out to $z = 1$. In all four plots shown, the five trendlines lie mostly within each others' error bars. Also, lower and higher redshift trendlines frequently cross each other. This suggests that the normalization factor is not redshift dependent out to $z = 1$.

In addition, the SIMBA plots in Figure 5 have two boxes at higher redshifts with extremely large standard deviations. In our data out to $z = 2$, similarly large standard deviations proliferate to the point where they compose a majority of our fits. They are also more common in the parameters other than the normalization factor at all redshifts. Upon inspection, these poor fits are due to overfitting—in these boxes, the data do not naturally follow a double power law. One remedy for this would be to choose a different fitting function. Until we complete that future step, we cannot draw satisfactory conclusions about redshift dependence for β, γ, or M_A, nor for the normalization factor out to $z = 2$.

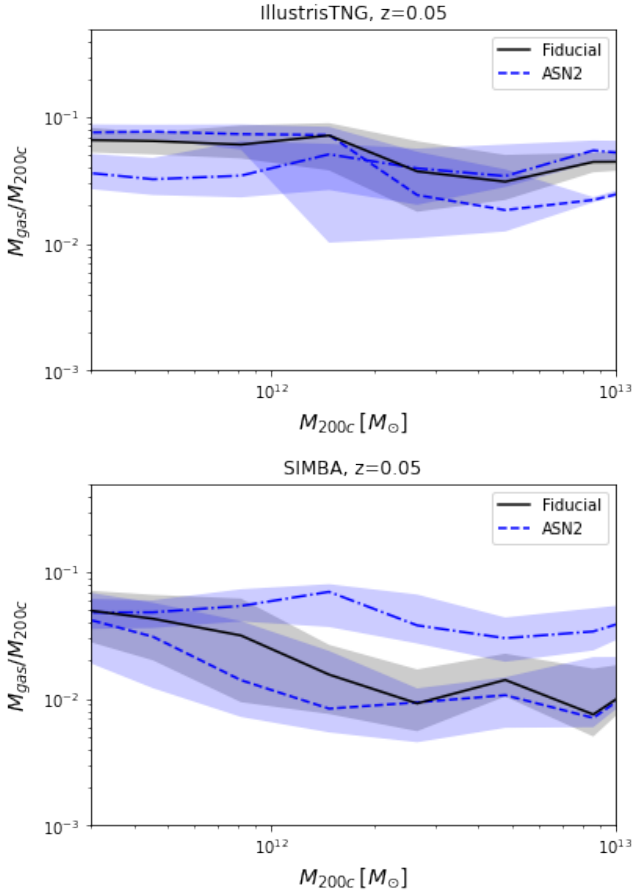

Figure 3. Each trendline shows the median GHMR in the fiducial 1P box and in the 1P boxes with lowest (dashed) and highest (dot-dashed) values of A_{SN2}. The scatter shows one standard deviation. Boxes run on IllustrisTNG exhibit an inflection point at a halo mass of around $10^{12.2} M_\odot$, while those run on SIMBA do not.

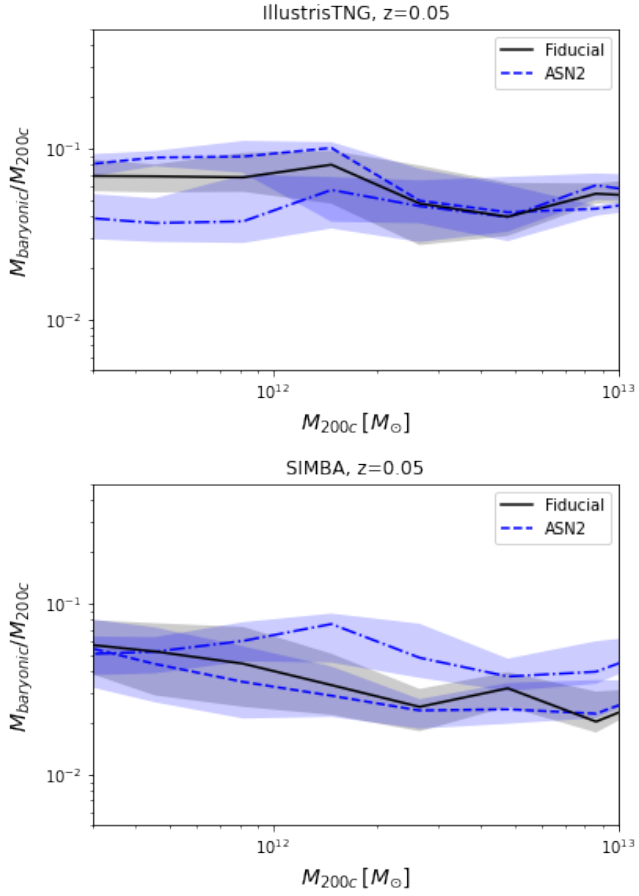

Figure 4. Each trendline shows the median BHMR in the fiducial 1P box and in the 1P boxes with lowest (dashed) and highest (dot-dashed) values of A_{SN2}. The scatter shows one standard deviation. Gas fractions dominate the baryonic portion of halos, but the stellar contribution shifts the high- and low-value trendlines closer to fiducial compared to gas.

ACKNOWLEDGEMENTS

Thank you to Dr. Priyanka Singh and Dr. Daisuke Nagai for mentoring me, to members of the x-emulator group for their ideas and advice, and to the Yale College First-Year Summer Research Fellowship in the Sciences and Engineering for funding this project.

DATA AVAILABILITY

The inclusion of a Data Availability Statement is a requirement for articles published in MNRAS. Data Availability Statements provide a standardised format for readers to understand the availability of data underlying the research results described in the article. The statement may refer to original data generated in the course of the study or to third-party data analysed in the article. The statement should describe and provide means of access, where possible, by linking to the data or providing the required accession numbers for the relevant databases or DOIs.

View all our figures here: https://drive.google.com/drive/folders/1zM793AHqqeklAfFIrimzGhauNcDtGS_x?usp=sharing.

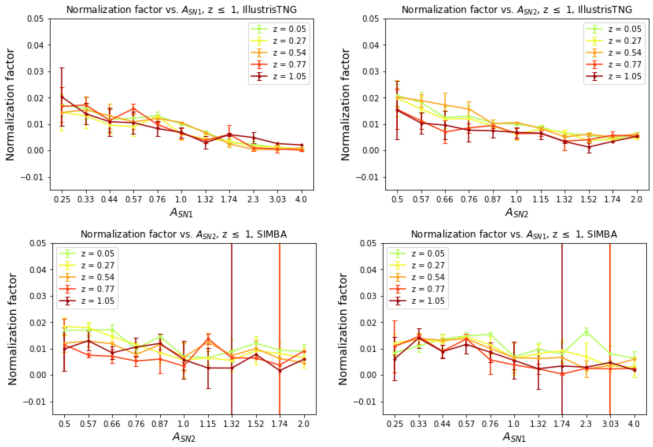

Figure 5. Each trendline follows the best-fit value for the normalization factor, A, in a double power law fit across 1P boxes with increasing values of A_{SN1} or A_{SN2}. The lines each correspond to a different redshift. The top panel shows IllustrisTNG; the bottom SIMBA.

REFERENCES

Villaescusa-Navarro F., Genel S., Anglés-Alcázar D., Perez L. A., Villanueva-Domingo P., Wadekar D., Shao H., et al., 2022, arXiv, arXiv:2201.01300
Girelli G., Pozzetti L., Bolzonella M., Giocoli C., Marulli F., Baldi M., 2020, A&A, 634, A135. doi:10.1051/0004-6361/201936329
Moster B. P., Somerville R. S., Maulbetsch C., van den Bosch F. C., Macciò A. V., Naab T., Oser L., 2010, ApJ, 710, 903. doi:10.1088/0004-637X/710/2/903

This paper has been typeset from a TEX/LATEX file prepared by the author.